(71) Applicant: KING ABDULLAH UNIVERSITY OF SCI-
ENCE & TECHNOLOGY [SA/SA]; King Abdullah Uni-
versity Of Science & Technology, 4700 King Abdullah
University Of Science & Technology, Thuwal, 23955-6900
(SA).

(72) Inventors: EL AFANDY, Rami Tarek; 4700 King Ab-
dullah University Of Science & Technology, Thuwal,
23955-6900 (SA). OOI, Boon Siew; 4700 King Abdullah
University Of Science & Technology, Thuwal, 23955-6900
(SA).

(74) Agent: PROCTOR, Ian; PROCTOR, Ian, 4700 King Ab-
dullah University Of Science & Technology, Thuwal,
23955-6900 (SA).

(54) Title: A HIGH-RESOLUTION, NANOMEMBRANE-BASED, THERMAL DIFFUSIVITY BIOSENSOR FOR LIVING CELLS
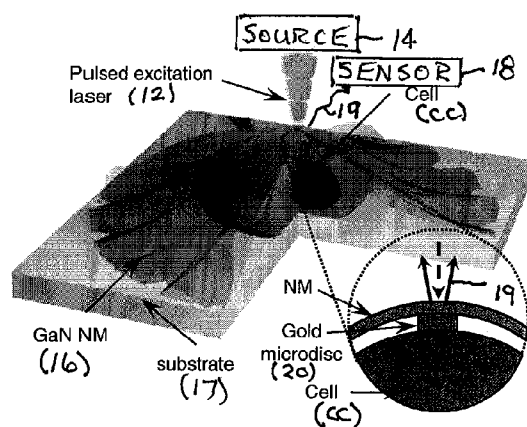
FIGURE 1

(57) Abstract: A method for measuring thermal diffusivity/conductivity of a microscale sample includes placing a metallic disk atop the sample, and disposing a nanomembrane over the sample and over the metallic disk so that the nanomembrane, so that the metal-lic disk, the nanomembrane and the sample are in thermal equilibrium with one another. A laser beam is directed to fall onto the nanomembrane over the sample, while a radiation sensor is operated to detect photoluminescent radiation emitted by the nanomembrane in response to the laser beam. A spectral shift in the detected photoluminescent radiation emitted by the nanomembrane is de-termined, and thermal diffusivity/conductivity is calculated from the determined spectral shift of the photoluminescence.

A HIGH-RESOLUTION, NANOMEMBRANE-BASED,
THERMAL DIFFUSIVITY BIOSENSOR FOR LIVING CELLS

BACKGROUND OF THE INVENTION

5

The present invention relates to a method for making high-resolution measurements of

biological (and non biological) thermal diffusivity and thermal conductivity. The resolution is such

that measurement of the thermal diffusivities/conductivities of individual biological cells is feasible

(Resolution can also reach sub-cell resolution (cell organels)). The present invention also relates to an

10   associated biosensor. In addition, the present invention relates to an associated kit facilitating

performance of the method.

With a 90 % mortality rate, cancer metastasis, or the spread of cancerous cells from a primary

tumor to seed secondary tumors, accounts for the majority of deaths among cancer patients[9,10].

Surgery, chemo-therapy and radiation-therapy, are ineffective in treating disseminated metastatic

15   cells[5]; however recent progress in functionalized magnetic and plasmonic nanoparticles has led

photothermal[3,4] and magneto-thermal[2] therapies to potentially target only cancerous cells throughout

the body. Because the cellular response to overheating is highly dependent on both the temperature

and the exposure time, and effects range from improved diffusion rate across the cellular membrane to

irreversible damage and protein denaturation[11], precise information regarding the transient thermal

20   energy distribution within the cell is required to efficiently target cancerous cells without affecting

adjacent healthy cells. In addition to cancer therapies, several imaging techniques, such as

photoacoustic[6,7] and photothermal[8] imaging, require the generation of confined heat pulses using

pulsed laser sources. Thus, cellular thermal diffusivity, as a measure of the transient thermal response

of a cell to a change in temperature, becomes a fundamental property to calculate the required

25   exposure time and intensity based on the requirements of the applications. Although there are standard

techniques for measuring thermal diffusivity, such as the transient plane or line sources and laser

flashing methods, they currently lack the spatial resolution needed to measure diffusivity at the

micron scale. Moreover, due to the irregular cellular curvilinear shapes, single-cell thermal diffusivity

measurement requires a flexible sensor that is capable of following their contours.

SUMMARY OF THE INVENTION

The ability to manipulate low dimensional physics phenomena within nanostructures has

5   always led to innovative techniques in determining physical properties of living cells, such as

electrical[12], optical[13] and mechanical[14,15]. Among the different nanostructures, 2D nanostructures, such

as nanomembranes (NMs), are unrivalled in their scalability for high-yield manufacture and, with the

current transfer techniques, are less challenging in their manipulation compared with lower-

dimensional nanostructures[16]. Furthermore, due to their extremely small flexural rigidity, NMs are

10   highly flexible and can follow curvilinear surfaces[17,18]. The operation principle of our novel technique

relies on the ability to spectrally shift the bandgap photoluminescence (PL) emission of gallium

nitride (GaN) NMs through laser-induced heating due to the increased phonons-boundary-scattering

rate. GaN NMs are just used for demonstration, other nanostructures or materials can be engineered to

perform the same functionality.

15   A method for measuring thermal diffusivity comprises, in accordance with the present

invention, (i) providing a microscale biological sample, (ii) placing a metallic disk atop the biological

sample, (iii) disposing a nanomembrane over the biological sample and over the metallic disc so that

the nanomembrane, the metallic disk and the biological sample are in thermal equilibrium with one

another, (iv) directing a laser beam to fall onto the nanomembrane over the biological sample, (v)

20   operating a radiation sensor to detect photoluminescent radiation emitted by the nanomembrane in

response to the laser beam, (vi) determining a spectral shift in the detected photoluminescent radiation

emitted by the nanomembrane, and (vii) calculating thermal diffusivity/conductivity from the

determined spectral shift of the photoluminescence.

Pursuant to a feature of the invention, the metallic disk is pre-attached to the nanomembrane.

25   The placing of the metallic disk and the disposing of the nanomembrane comprise positioning the

nanomembrane and the metallic disk together atop the biological sample. Typically, the

nanomembrane is provided with the metallic disk lying thereon, so that the method further

contemplates flipping the nanomembrane so that the disk is underneath. The positioning of the

nanomembrane and the metallic disk is performed after the flipping of the nanomembrane.

Another feature of the invention is without the usage of a metallic disk. In this case, the NM

5   is formed from a material which can be excited with a wavelength that is not absorbed by the

underlying biological (or non-organic) material.

Pursuant to another feature of the invention, a kit for use in making measurements of thermal

diffusivity of microscale biological material comprises at least one nanomembrane having a

maximum edge dimension in a microscale range and at least one metallic disk having a maximum

10   dimension substantially less than a smallest dimension of the nanomembrane. The term "microscale"

is used herein to denote sizes on the same order as that of living cells and clumps of cells. The

nanomembranes are typically so small that a microscope is required to enable manipulation by a user.

The kit preferably comprises a plurality of nanomembranes each having a maximally sized

edge dimension in a microscale range and further comprises a plurality of metallic disks each having a

15   maximum dimension substantially less than a smallest dimension of each of the nanomembranes.

Where the metallic disks are circular, they may have a diameter of between one half and one-

twentieth that of an edge of a square nanomembrane.

The disks are preferably made of a material taken from the group consisting of gold, a gold

alloy, platinum, and a platinum alloy, Aluminum, Silver (many of the metals will function at different

20   wavelengths) and are each fastened to a respective one of the nanomembranes.

The present invention provides a method and apparatus for measuring single-cell thermal

diffusivity. Here, the present approach approach of measuring the thermal diffusivity of single-cells

has only a 2.2% error rate. We base our technique on increasing the diffusive phonon-boundary-

scattering rate in nanomembranes to induce a considerable spectral dependence of the excitonic-

25   bandgap emission over excitation-laser intensity. We further demonstrate that once in contact with

organic or inorganic material, the nanomembranes' emission spectral-shift functions as an indicator of

the material's thermal diffusivity. Due to the prior absence of a single-cell thermal diffusivity sensor,

we anticipate our novel technique to enable an efficient single-cell targeting using nanoheaters, allow

better modeling of thermal distribution within cells and potentially enable novel diagnostic techniques

based on variations of single-cell thermal diffusivities.

5

BRIEF DESCRIPTION OF THE DRAWINGS

Figure 1 is a schematic perspective view of a biosensor assembly for measuring single-cell

thermal diffusivity. Schematic representation of a cell attached to a substrate and covered with a GaN

NM. A laser beam is focused on the NM to induce local heating as well as PL emission. Because heat

10   spontaneously diffuses from the NM to the cell, the temperature of the NM depends on the cell

thermal diffusivity. Consequently, based on the measured temperature-dependent PL emission from

the NM, we can estimate the cell thermal diffusivity. The magnified region represents the focused

excitation beam (dashed arrow), which simulates spontaneous bandgap emission (straight solid

arrows) as well as local heat energy which diffuses away from the source (zigzagged arrows).

15   **Figures 2a** through **2e** pertain to intensity-dependent PL emissions from NMs. **Figure 2a** is a

band diagram of the photo-excited free-excitons in GaN showing laser excitation, phonon-assisted

relaxation and PL emission.   **Figure 2b** is a schematic perspective view showing a nanomembrane

disposed on a copper grid and exposed to a laser beam, to measure the laser-induced local heating.

Figure 2c is an optical image of the structure shown in Figure 2b.   **Figure 2d** is a pair of graphs

20   showing that, with increasing laser excitation intensity, PL signals measured from 40 and 10 nm thick

GaN NMs exhibited spectral redshifts of different magnitudes because of the decrease of the thermal

conductivity with NM thickness. **Figure 2e** is a graph showing thermal conductivity simulation

results of the laser-induced heating within the NMs. Circles, squares and triangles represent the mean

measured peak emission energy from the 40, 20 and 10 nm thick NMs, respectively. The simulation

25   results are indicated by solid black curves. An inset 3D plot shows the simulated steady-state heat

distribution across the NM.

Figures 3a through 3d show COMSOL Multiphysics simulation results of the temperature profile due to a 100 µs long excitation laser pulse. **Figure 3a** is a schematic two-dimensional diagram of temperature distribution within a cell when the NM is in direct contact with the cell. **Figure 3b** is a schematic two-dimensional diagram of temperature distribution within a cell when a

5   250 nm thick Au film is inserted under the NM. **Figure 3c** is a schematic two-dimensional diagram of temperature distribution within a cell when the Au film is reduced to a 3 µm wide microdisk. The insertion of an Au film causes rapid lateral diffusion of the heat energy within the film. When the film is reduced to a disk, lateral heat diffusion is suppressed and heat diffuses vertically from the NM to the cell. **Figure 3d** is a graph showing a simulated temperature depth profile for the three cases of

10   Figures 3a-3c due to a 100 µs long excitation pulse, with the lowest curve corresponding to Figure 3a (no gold), the middle curve corresponding to Figure 3b (gold film) and the upper curve corresponding to Figure 3c (gold microdisk). While the Au film caused a severe drop in the temperature, due to the enhanced lateral diffusion, temperature depth profile for the direct contact and the Au disk cases are similar. Ambient temperature was taken as 37°C in these simulations.

15   Figures 4a through 4e show experimental measurements of thermal diffusivity. **Figure 4a** is an optical microscope image of the GaN NMs with the Au microdisk attached while resting on their original GaN substrate. **Figure 4b** is an image showing a 10 µm wide tungsten tip used in picking up individual NMs from the GaN substrate, flipping them, transferring them to different materials. **Figure 4c** shows an NM as transferred onto a substrate. With the NM facing downwards, the Au

20   microdisk was sandwiched between the NM and the foreign substrate. **Figure 4d** is an SEM micrograph of a cancer cell covered by a 35 nm thick NM. The micrograph is imaged under high KV mode to make the Au microdisk apparent in the image. **Figure 4e** is a plot of the temperature difference ratios of the NM of several materials versus their thermal diffusivities (black dots). The solid curve is the same ratio constructed from the analytical solution to the heat diffusion equation 2.

25   The positively sloped linear plot is the calculated measurement resolution.

Figure 5 is a diagram of an experimental setup used to measure thermal diffusivities. The diagram depicts an beam optical path for an excitation 325 nm laser as well as PL emission from target NMs.

Figure 6 is a pair of graphs showing PL emission from a nanomembrane attached to a cell.

5   Collected PL emissions from a single NM attached to a cell at an increasing laser excitation intensity for long (top graph) and short (bottom graph) pulse widths.

DETAILED DESCRIPTION

As illustrated in   **Figure 1**, a pulsed, focused laser beam 12 from a laser source 14

10   locally heats a gallium nitride nanomembrane (NM) 16 that is in direct contact with a cancer cell CC disposed on a substrate 17. The generated heat energy spontaneously diffuses to the cancer cell CC at a rate proportional to the cell's thermal diffusivity. The temperature of the NM 16 thus depends on the cell's thermal diffusivity. A light sensor 18 such as a photocell or solid state camera (charge coupled device or CCD) detects photoluminescent (PL) light emission 19 from the nanomembrane

15   NM. Knowledge of the nanomembrane's temperature, obtained by measuring the spectral-shift in its PL emission, yields information of the thermal diffusivity of the cancer cell CC. A gold microdisk 20 is disposed between and in thermal contact with the NM 16 and the cancer cell CC. The function of the gold (Au) microdisk 20 is to block unabsorbed laser radiation to prevent it from being absorbed within the underlying cell CC as further explained below. Because GaN is a robust, chemically stable

20   and biocompatible[19] material we selected GaN material for the NM 16. Although fabrication of GaN NMs of different dimensions and crystalline properties has been demonstrated by several groups[20-22], there is no published work on employing their properties for biomedical applications.

Laser-induced heating in GaN NMs

25   Prior to demonstrating thermal diffusivity measurements of single-cells with the GaN NMs, it is imperative to study the effect of laser-induced local heating on the PL emission from NMs. Once

excited by a 325 nm (3.81 eV) continuous-wave laser, photo-excited free-excitons emit a series of

optical and acoustic phonons while relaxing towards their energy band minimum to conserve energy

and momentum simultaneously (**Figures** 2a)[23]. Thus, a local non-equilibrium density of

phonons (a non-equilibrium temperature gradient) is established, causing the phonons to

5   spontaneously diffuse away from the excitation region into the surrounding crystal. Due to its long

phonon mean free path, or average distance travelled before scattering, $(\Lambda_{ph} \sim 100 \text{ nm })^{24}$, GaN

thermal conductivity is sufficiently high $(\kappa_{GaN} = 227 \text{ W/m.K})^{25}$ which enables rapid phonon

diffusion. Therefore, no steady-state local increase in temperature occurs, and the GaN PL peak

emission energy (3.42 eV) exhibits no spectral dependence over increasing excitation laser intensity

10   (up to 4.84 $\frac{mW}{\mu m^2}$). Although phonon scattering in bulk GaN crystal at room temperature is

dominated by Umklapp processes[26], once the crystal is reduced to a NM structure, with a thickness of

less than Λ_{ph}, diffusive phonon-boundary-scattering becomes dominant and causes a reduction in Λ_{ph}

to approximately the NM thickness $(W_{NM})^{27}$. Consequently, the GaN NM thermal conductivity

$(\kappa_{NM} \propto \Lambda_{ph})$ significantly reduces as it scales down with W_{NM}[28]. Therefore, thermal energy is not

15   dissipated rapid enough, and a steady-state increase in local temperature is established, which causes

the GaN PL peak emission to redshift with increasing laser excitation intensity.

To measure the PL emission from the GaN NMs, we transferred the GaN NMs 16 to a copper

grid 22, and focused a 325 nm laser beam 12 onto the NMs to a 3 μm spot size, as schematically

presented in   Figures 2b and optically imaged in   Figures 2c. The normalized PL emissions

20   from 40 and 10 nm thick GaN NMs at increasing laser excitation intensities were measured and

plotted in   Figures 2d. At low-excitation intensity (3.3 $\frac{\mu W}{\mu m^2}$), all NMs, regardless of

thicknesses, emitted at the same energy (3.42 eV), indicating the absence of laser-induced local

heating. However, at increasing excitation intensities, thinner NMs exhibited longer red-shifts as well

as wider full width at half maximums (FWHMs), which is ascribed to an increase in the local

25   temperature due to the increased probability of phonon-boundary-scattering[29,30].

To quantitatively estimate κ_{NM} based on the spectral shift, we numerically solved the steady-state heat equation using MATLAB and then fitted the experimental data. Using the following equation:

$$-\kappa_{NM} W_{NM} \nabla^2 T + h_{tot}(T - T_a) + \epsilon \sigma_{SB}(T^4 - T_a^4) - Q_{exc}(x, y),$$ (1)

5   where T and T_a are the NM and ambient temperatures, respectively. h_{tot}, ϵ and σ_{SB} are the

convection heat transfer coefficient, the GaN emissivity and the Stefan-Boltzmann constant,

respectively. Finally, $Q_{exc}(x, y)$ is the heat generated within the NM due to excitation laser, modelled

by a Gaussian distribution. The simulated steady-state heat distribution across the NM, plotted in the

inset of   Figures 2e, indeed showed a steady-state accumulation of heat energy centred on the

10   excitation laser spot. The PL emission energy from the NM was calculated from the local temperature

based on Varshni's equation[31]. The mean measured peak emission energies were plotted with

increasing excitation intensities in   Figures 2e for 40, 20 and 10 nm thick NMs, presented by circles,

squares and triangles, respectively. κ_{NM} of 20.5, 15.4 and 9 W/m.K gave the best simulation fit to the

experimental data for the 40, 20 and 10 nm thick NMs, respectively.

15   **Thermal diffusivity sensing design**

In our attempt to establish a solid theoretical foundation for our novel NM-based thermal

diffusivity sensing technique, we first find an analytical solution to the heat diffusion equation. We

simplified our NM/cell system to a semi-infinite homogenous medium which had an adiabatic surface

and was heated by a Gaussian heat source. The rise in peak temperature at the heating source (at the

20   NM) is then given by,

$$\Delta T(t) - A \frac{\sigma^2}{\kappa_{cell}} \times \left(\frac{1}{\sigma} - \frac{1}{\sqrt{\sigma^2 + 2\alpha_{cell}t}} \right),$$ (2)

where A and σ are the Gaussian heat source (laser) amplitude and standard deviation, respectively;

κ_{cell} and α_{cell} are the cell thermal conductivity and diffusivity, respectively; and t represents the

heating time[32]. It is apparent from the above solution that the NM emission, as a function of ΔT,

depends on both κ_{cell} and α_{cell} which should not be the case for a thermal diffusivity measurement technique. However, the ratio of the temperature changes due to different heating

periods, $R_{t_1/t_2} = \frac{\Delta T(t_1)}{\Delta T(t_2)}$, cancels the time-independent term outside the bracket and is only a function of α_{cell}. Thus, instead of using a continuous laser source, the laser was pulsed at two

5   different time periods (t_1 and t_2), and the ratio between the rise in local temperatures was calculated. This technique also allowed the measurement to be independent from the laser amplitude, which yielded a more controlled experiment.   **Figures** *3*a shows the COMSOL Multiphysics simulation results of the heat diffusion equation within the NM/cell system due to a 100 μs long laser pulse, with the temperature depth profile plotted in   Figures *3*b, red curve (simulation details are

10   provided in the Supplementary Information). As demonstrated from the depth profile, a 100 μs long pulse width limited the heat diffusion to within the cell boundaries, thus allowing for the infinite medium approximation.

Because the NM thickness used in this study (35 nm) was much less than the penetration depth of 325 nm radiation in GaN (~ 85 nm), approximately 50% of the optical energy was

15   transmitted through the NM. This transmitted energy, depending on the underlying cell's optical properties, was absorbed, transmitted or reflected back to the NM. Therefore, the generated heat energy, and hence the observed PL energy shift, became functions of the cell's optical properties. To address this issue, we inserted a 250 nm thin layer of Au under the NM to prevent UV radiation from reaching the cancer cell, while at the same time, due to its high thermal diffusivity (170 mm^2/s), does

20   not interfere with heat diffusion from the NM to the cancer cell. Unfortunately, as demonstrated by the simulation results (Figures *3*b and the blue curve in   Figures *3*d), the insertion of an Au film significantly enhanced lateral thermal diffusion, which delocalized the generated heat energy and rendered the measurements prone to boundary effects (such as cell dimensions and surrounding medium). To suppress lateral thermal diffusion, the Au film was reduced to a 4 μm wide microdisk (

25   Figures *3*c). The modified temperature profile became similar to the direct contact case with a considerable increase in temperature due to the absorbed laser energy within the Au microdisk.

Thermal diffusivity measurement

To verify the ability of the described experimental design to measure thermal diffusivity, we first transferred the NMs to several materials of known thermal diffusivities ($\alpha_{material}$) and recorded $R_{t_2}^{t_1}$. Through several lithography, metal evaporation and plasma etching techniques, we

5   fabricated 40 μm wide, 35 nm thick GaN NMs with 3 μm wide, 250 nm thick Au microdisks attached to them (**Figures 4**a and Methods). With the aid of a 10 μm tungsten tip attached to a micrometre probe positioner, we picked up the NMs (Figures 4b, video in Supplementary Information), flipped them (so that the Au microdisk is facing down) and transferred them to several materials with different $\alpha_{material}$ (Figures 4c). To eliminate any structural or morphological

10   variations within the NMs and the attached Au microdisks, which would induce errors within the measurements, we only transferred adjacent NMs from an area of 0.5x0.5 mm^2. A 325 nm pulsed laser was focused onto the Au microdisk and the PL emission was measured at increasing laser intensities. The increase in the NM local temperature was then calculated from the PL shift using Varshni's equation. Finally, the measurement was repeated at two different laser pulse widths (100

15   and 6 μs), and $\frac{R_{100}}{6}$ was calculated for the NMs on the different materials ($\frac{R_{100}}{6}$ is plotted versus $\alpha_{material}$ Figures 4e, black circles). The solid hyperbolic curve in Figures 4e represents the analytical solution (equation 2) using the current experimental conditions (Methods). Although, similar dependence of $\frac{R_{100}}{6}$ over $\alpha_{material}$ is observed at both the experimental and analytical solutions, higher $\frac{R_{100}}{6}$ values are analytically calculated than experimentally measured at

20   lower $\alpha_{material}$. This discrepancy arose because the analytical solution did not account any heat loss from the NM surface, whether convection or radiation.

Next we demonstrate the applicability of our technique to biological cells. First, we constructed a calibration curve (red dotted curve in Figures 4e) from the experimental data to estimate α_{cell} given $R_{100,6}$. We observe a clear nonlinearity in the sensitivity of our measuring

25   technique, given by the slope of the calibration curve ($\delta R_{t_1,t_2}/\delta\alpha$, where δ denotes the minimum

resolution of the quantity), with the sensitivity improving with decreasing $\alpha_{material}$. We then plated

an MCF-7 breast cancer cell line onto a glass slide (Methods), and with the aid of a tungsten tip, we

performed multiple transfers of NMs on top of several cells (Figures *4*d). From several cells of

the same cell line, we measured an average $\frac{R_{100}}{6}$ equal to 2.05 (Supplementary Information), which

5   yielded α_{cell} equal to 0.123 mm²/s. Interestingly, the measured α_{cell} was slightly less than that of

water (0.143 mm²/s), which is consistent with the fact that water normally accounts for approximately

80 % of the cell's weight. Furthermore, the water content within living cells harbors a large

composition of macromolecules, such as proteins, having calculated thermal conductivities less than

water[33,34], thereby contributing to a lower thermal conductivity of living cells[35].

10   The measurement resolution of our thermal diffusivity measuring technique ($\delta\alpha$) is limited by

experimental setup as well as by measured sample properties. Over the range of 3.33 eV to 3.42 eV,

the average spectral resolution of the 2400 lines grating (δE_{GR}) used in the above measurements is

0.137 meV, which yields a value of 0.25°C for δT. Because

$$\delta R_{t_1,t_2} = R_{t_1,t_2}\sqrt{\left(\delta T/\Delta T_1\right)^2 + \left(\delta T/\Delta T_2\right)^2}$$, we observe that higher temperature shifts, which depend

15   on $\kappa_{material}$, A_{laser} and σ_{laser}, result in smaller $\delta R_{t_1,t_2}$. Based on the optics and materials used

(Supplementary Information), we plot the calculated $\delta R_{t_1,t_2}$ (green curve in   Figures *4*e). As

$\alpha_{material}$ decreases, $\delta R_{t_1,t_2}$ decreases from 0.026 (for silicon) to 0.014 (for parylene) with a value of

0.019 for the MFC-7 cancer cells. Using $\delta R_{t_1,t_2}/\delta\alpha$, we obtain $\delta\alpha_{cell}$ = 0.0026 mm²/s, which is only

2.2% of the measured α_{cell}. Increasing the laser intensity or the pulse width lowers this error but on

20   the expense of generating more heat which will affect the cancer cells. On the other hand, using

materials with optical emissions which have higher spectral dependence over temperature than GaN,

will increase the measuring resolution of the technique.

In conclusion, we developed a novel thermal diffusivity measuring technique based on the

transient response of GaN NMs to laser-induced heating. We also successfully measured, for the first

time, the thermal diffusivity of cancerous cells to enable high-precision single-cell targeting using
nanoparticles based hyperthermia treatment. Moreover, measuring the thermal diffusivities yields a
more controllable experimental design for therapeutic or imaging techniques dealing with transient
temperature variations within the cells. While we measured diffusivity for single cells, the spatial
5   resolution can be increased or decreased, with a shorter or longer pulse width, respectively, to
measure the diffusivity of subcellular regions or cell clusters and whole tissues. Finally, as
demonstrated, the presented technique is not limited to biomedical applications and can also be
employed in non-biological samples.

Methods

10   **NM fabrication.** Using a VEECO GEN930 plasma-assisted molecular beam epitaxy (PAMBE)
system, a 35 nm thick indium gallium nitride (InGaN) sacrificial layer was grown at 560°C, followed
by 40 nm thick GaN grown at 640°C, on a 500 nm GaN on a sapphire template wafer. The wafer was
then cleaved into 1 **cm²** pieces, which were subsequently degreased in acetone and isopropanol (IPA)
for 5 mins and then cleaned in nitric acid (HNO_3) at 65°C for 15 mins for surface oxide removal. A
15   thin layer of platinum metal (150 nm) was then deposited near the edge of the top surface. Finally, a
layer of AZ resist was spin-coated and patterned into 40 μm wide disks, followed by inductively
coupled plasma (ICP) reactive ion etching (RIE) using an Argon (Ar)/Chlorine (Cl)-based recipe to
expose the InGaN sacrificial layer. The remaining photoresist was then removed with acetone, and the
sample was cleaned in IPA.

20   **Au microdisk fabrication.** A 250 nm thick layer of Au was evaporated onto the sample, followed by
a spin-coated layer of SU8-2000.5 photoresist which was then patterned into 4 μm disks. Using Ar-
bombardment in an ICP reactor, 150 nm of Au was removed, followed by 10 seconds immersion in
potassium iodide (KI)/ iodine (I_2) based Au etchant to etch away the remaining 100 nm, leaving
behind the intact GaN structure. Finally, oxygen (O_2) plasma was used to remove the remaining SU-8
25   photoresist.

NM exfoliation. The samples were immersed in a bath containing $CH_3OH: H_2O_2 (35\%): HF (49\%)$

(1:2:2). Back light illumination was performed by focusing light coming from a 200 W mercury (Hg)

arc lamp onto the sample. To selectively etch the InGaN sacrificial layer, any photon energies higher

than the GaN bandgap was blocked by placing a polished GaN wafer on top of the etching bath[36].

5   Once the InGaN was completely etched, the samples were gently cleaned by dipping them in IPA and

were then dried using a critical point dryer (CPD) to enable proper exfoliation of the NM.

PL measurement. The PL emission from the NM was measured by focusing radiation from a helium-

cadmium (He-Cd) gas laser to an average spot of $3\,\mu m$ in diameter. The PL signal was then collected

and sent to a 2400 line diffraction grating for dispersion. We pulsed the laser by passing the beam

10   through a high-speed chopper. (More details are described in the Supplementary Information)

Cell culture. Breast cancer cell lines (MCF-7) were purchased from ATCC (Manassas, VA, USA).

The MCF-7 cells were cultured in MEM medium supplemented with 10% foetal bovine serum (FBS)

and Penicillin/Streptomycin solution (100 units/ml penicillin, 100 µg/ml streptomycin) and

maintained in a humidified incubator at 37°C and 5% CO_2. In all assays, the cells used were from

15   passages 5-25 and were used in suspension or plated on a glass slide (Fisher Scientific Ltd, UK) pre-

coated with attachment factor protein (1X; Fisher Scientific Ltd, UK) for 30 minutes at 37°C. Finally,

the MCF-7 cells were seeded at a density of 3×10^5 cells/mL (9×10^4 cells/cm^2) and incubated at

37°C and 5% CO_2 in a humidified incubator for 24 hours before transferring the NMs onto the cells.

COMSOL Multiphysics simulation. The cell was modelled as a cylinder with a 5 µm radius and a

20   10 µm height. Because water normally accounts for approximately 80 % of the cell's weight, we used

water thermal conductivity and diffusivity to model the thermal properties of living cells. Because

cells have even lower thermal diffusivities than water, heat energy will be further confined in case of

cells. Regarding the thermal properties of gallium nitride (GaN) and gold (Au), we used the values

available in the COMSOL libraries. The following time-dependent heat diffusion equation was solved

25   for the NM/Au microdisk/cell system:

$$\frac{\partial T}{\partial t} + VT = V.(\alpha VT) + \frac{Q}{\rho C_p}$$

where α, ρ, C_p and Q are the thermal diffusivity, density, specific heat capacity at constant pressure and heat source power per unit volume, respectively. The initial temperature was set at 37 °C. Convection cooling from the NM is taken into account by having a column of air on the NM.

5   **Experimental optical setup.** As shown in **Error! Reference source not found.**5, 325 nm laser radiation, originating from a helium-cadmium (He-Cd) laser 50, was first chopped into 6 µs or 100 µs pulses using a Scitec 310CD high-speed optical chopper 52 with an in-house drilled 400 µm wide hole 54. The generated pulses 56 had a very low duty cycle (1.27×10^{-3}) to ensure that all of the laser-generated heat energy during one pulse is dissipated before the incoming second heating pulse. A set

10   of optical density filters 58 were used to vary the laser radiation intensity from 0.027 to 1.235 mW/µm². After locating the Au microdisk (not shown), which is attached to the NM 58, the laser beam pulses 56 were reflected by a beam splitter 60 and focused to a spot of 3 µm in diameter using a 40x UV objective lens 62. The sample 64 was left on a thermo-electric controller 66, set at 37 °C, long enough to reach thermal equilibrium prior to performing the measurement. The

15   photoluminescence emission 68 from the NM 58, was then collected by the same objective 62, transmitted through the beam splitter 60, filtered at 70 and dispersed by a 2400 line grating 72 onto a charge-coupled device (CCD) camera 74. Each measurement consisted of collecting the PL emission at different laser radiation intensities and different chopping speeds.

Materials used for calibration

20   Prior to measuring the thermal diffusivities of cells, we transferred the NMs onto materials of known thermal diffusivities to calibrate the measured signal. Because the fabrication/growth procedure of any material affects its final thermal diffusivity, we could not rely on standard available thermal diffusivities and had to measure the thermal diffusivities ourselves. The measured thermal diffusivities of the materials, which were measured using laser flash technique, are listed in

25

Error! Reference source not found..

Material	Thermal diffusivity (mm^2/s)
Parylene	0.0588
Poly(methyl methacrylate) (PMMA)	0.09
Polyether ether ketone (PEEK)	0.178
Soda-lime glass	0.487
Quartz	0.78
Sapphire	8.77
Silicon	80

Table 1

Heating curves of a single cell

5   Error! Reference source not found.10 shows a sample of the measured PL emissions from NMs on
cells. At both long (100 µs) and short (6 µs) pulse widths, the PL emission from the NM attached to
the cancer cell emitted at the same peak emission when the excitation intensity was 0.027 mW/µm^2.
As the excitation intensity increased, the PL emission from the NM got spectrally redshifted due to
the laser-induced heating. As observed, the redshift was higher for a 100 µs pulse width than a 6 µs
10   pulse. We then converted the energy shifts into temperature shifts (using Varshni's equation). Finally,
the ratio between the two shifts was calculated and used to estimate the thermal diffusivities (using
the calibration curve constructed above, Figure 4).

15   REFERENCES

1   Steeg, P. S. Tumor metastasis: mechanistic insights and clinical challenges. *Nat Med* **12**, 895-
904 (2006).

2   Lee, J.-H. *et al.* Exchange-coupled magnetic nanoparticles for efficient heat induction. *Nat
Nano* **6**, 418-422, doi:10.1038/nnano.2011.95 (2011).

20   3   Chen, J. *et al.* Gold Nanocages as Photothermal Transducers for Cancer Treatment. *Small* **6**,
811-817, doi:10.1002/smll.200902216 (2010).

4   Stephan Link, M. A. E.-S. Shape and size dependence of radiative, non-radiative and photothermal properties of gold nanocrystals. *International Reviews in Physical Chemistry* **19**, 409-453, doi:10.1080/01442350050034180 (2010).

5   Schroeder, A. *et al.* Treating metastatic cancer with nanotechnology. *Nat Rev Cancer* **12**, 39-50 (2012).

6   Zhang, H. F., Maslov, K., Stoica, G. & Wang, L. V. Functional photoacoustic microscopy for high-resolution and noninvasive in vivo imaging. *Nat Biotech* **24**, 848-851, doi:10.1038/nbt1220 (2006).

7   Jathoul, A. P. *et al.* Deep in vivo photoacoustic imaging of mammalian tissues using a tyrosinase-based genetic reporter. *Nat Photon* **9**, 239-246, doi:10.1038/nphoton.2015.22 (2015).

8   Zharov, V. P. & Lapotko, D. O. Photothermal imaging of nanoparticles and cells. *Selected Topics in Quantum Electronics, IEEE Journal of* **11**, 733-751, doi:10.1109/JSTQE.2005.857382 (2005).

9   Mehlen, P. & Puisieux, A. Metastasis: a question of life or death. *Nat Rev Cancer* **6**, 449-458 (2006).

10   Society, A. C. Cancer Facts & Figures 2014. *Atlanta: American Cancer Society* (2014).

11   Habash, R. W. Y., Bansal, R., Krewski, D. & Alhafid, H. T. Thermal Therapy, Part 2: Hyperthermia Techniques. *Critical Reviews in Biomedical Engineering* **34**, 491-542, doi:10.1615/CritRevBiomedEng.v34.i6.30 (2006).

12   Duan, X. *et al.* Intracellular recordings of action potentials by an extracellular nanoscale field-effect transistor. *Nat Nano* **7**, 174-179, doi:10.1038/nnano.2011.223 (2012).

3   Choi, W. J. *et al.* Full-field optical coherence microscopy for identifying live cancer cells by quantitative measurement of refractive index distribution. *Opt. Express* **18**, 23285-23295, doi:10.1364/OE.18.023285 (2010).

14   Hénon, S., Lenormand, G., Richert, A. & Gallet, F. A new determination of the shear modulus of the human erythrocyte membrane using optical tweezers. *Biophysical Journal* **76**, 1145-1151 (1999).

15   Hanson, L. *et al.* Vertical nanopillars for in situ probing of nuclear mechanics in adherent cells. *Nat Nano* **10**, 554-562, doi:10.1038/nnano.2015.88 (2015).

16   Rogers, J., Lagally, M. & Nuzzo, R. Synthesis, assembly and applications of semiconductor nanomembranes. *Nature* **477**, 45-53 (2011).

17   Viventi, J. *et al.* A Conformal, Bio-Interfaced Class of Silicon Electronics for Mapping Cardiac

        Electrophysiology. *Science Translational Medicine* **2**, 24ra22-24ra22,

        doi:10.1126/scitranslmed.3000738 (2010).

18   Chae, S. H. *et al.* Transferred wrinkled Al2O3 for highly stretchable and transparent

        graphene–carbon nanotube transistors. *Nature Materials* (2013).

19   Jewett, S. A., Makowski, M. S., Andrews, B., Manfra, M. J. & Ivanisevic, A. Gallium nitride is

        biocompatible and non-toxic before and after functionalization with peptides. *Acta

        Biomaterialia* **8**, 728-733, doi:10.1016/j.actbio.2011.09.038 (2012).

20   Mei, Y. *et al.* Fabrication, Self-Assembly, and Properties of Ultrathin AlN/GaN Porous

        Crystalline Nanomembranes: Tubes, Spirals, and Curved Sheets. *ACS Nano* **3**, 1663-1668,

        doi:10.1021/nn900580j (2009).

21   ElAfandy, R. T. *et al.* Exfoliation of Threading Dislocation-Free, Single-Crystalline, Ultrathin

        Gallium Nitride Nanomembranes. *Advanced Functional Materials* **24**, 2305-2311,

        doi:10.1002/adfm.201303001 (2014).

22   Tiginyanu, I., Popa, V. & Stevens-Kalceff, M. A. Membrane-assisted revelation of the spatial

        nanoarchitecture of dislocation networks. *Materials Letters* **65**, 360-362,

        doi:10.1016/j.matlet.2010.10.033 (2011).

23   Kovalev, D. *et al.* Free exciton emission in GaN. *Physical Review B* **54**, 2518-2522 (1996).

24   Danilchenko, B. A., Paszkiewicz, T., Wolski, S., Jeżowski, A. & Plackowski, T. Heat capacity and

        phonon mean free path of wurtzite GaN. *Applied Physics Letters* **89**, 061901,

        doi:10.1063/1.2335373 (2006).

25   Slack, G. A., Schowalter, L. J., Morelli, D. & Freitas Jr, J. A. Some effects of oxygen impurities

        on AlN and GaN. *Journal of Crystal Growth* **246**, 287-298, doi:10.1016/S0022-

        0248(02)01753-0 (2002).

26   Zou, J., Kotchetkov, D., Balandin, A. A., Florescu, D. I. & Pollak, F. H. Thermal conductivity of

        GaN films: Effects of impurities and dislocations. *Journal of Applied Physics* **92**, 2534-2539,

        doi:10.1063/1.1497704 (2002).

27   Aksamija, Z. & Knezevic, I. Anisotropy and boundary scattering in the lattice thermal

        conductivity of silicon nanomembranes. *Physical Review B* **82**, 045319 (2010).

28   Klitsner, T. & Pohl, R. O. Phonon scattering at silicon crystal surfaces. *Physical Review B* **36**,

        6551-6565 (1987).

29   Guthy, C., Nam, C.-Y. & Fischer, J. E. Unusually low thermal conductivity of gallium nitride

        nanowires. *Journal of Applied Physics* **103**, 064319, doi:10.1063/1.2894907 (2008).

30   Piscanec, S. *et al.* Raman spectroscopy of silicon nanowires. *Physical Review B* **68**, 241312 (2003).

31   Nepal, N., Li, J., Nakarmi, M. L., Lin, J. Y. & Jiang, H. X. Temperature and compositional dependence of the energy band gap of AlGaN alloys. *Applied Physics Letters* **87**, -, doi:10.1063/1.2142333 (2005).

32   Antonakakis, T., Maglioni, C. & Vlachoudis, V. Closed form solutions of the heat diffusion equation with a Gaussian source. *International Journal of Heat and Mass Transfer* **62**, 314-322, doi:10.1016/j.ijheatmasstransfer.2013.02.061 (2013).

33   Müller, T. J. & Müller-Plathe, F. Heat transport through a biological membrane—An asymmetric property? Technical issues of nonequilibrium molecular dynamics methods. *International Journal of Quantum Chemistry* **111**, 1403-1418, doi:10.1002/qua.22785 (2011).

34   Yu, X. & Leitner, D. M. Heat flow in proteins: Computation of thermal transport coefficients. *The Journal of Chemical Physics* **122**, 054902, doi:10.1063/1.1830431 (2005).

35   Kyoo Park, B., Yi, N., Park, J. & Kim, D. Thermal conductivity of single biological cells and relation with cell viability. *Applied Physics Letters* **102**, -, doi:10.1063/1.4807471 (2013).

36   Stonas, A. R., Margalith, T., DenBaars, S. P., Coldren, L. A. & Hu, E. L. Development of selective lateral photoelectrochemical etching of InGaN/GaN for lift-off applications. *Applied Physics Letters* **78**, 1945, doi:10.1063/1.1352663 (2001).

WHAT IS CLAIMED IS:

1. A method for measuring thermal diffusivity/conductivity, comprising:

providing a microscale biological sample;

placing a metallic disk atop the biological sample;

disposing a nanomembrane over the biological sample and over the metallic disc so that the

nanomembrane, the metallic disk and the biological sample are in thermal equilibrium with one

another;

directing a laser beam to fall onto the nanomembrane over the biological sample;

operating a radiation sensor to detect photoluminescent radiation emitted by the

nanomembrane in response to the laser beam;

determining a spectral shift in the detected photoluminescent radiation emitted by the

nanomembrane; and

calculating thermal diffusivity/conductivity from the determined spectral shift of the

photoluminescence.

2. The method defined in claim 1 wherein the metallic disk is attached to the

nanomembrane, the placing of the metallic disk and the disposing of the nanomembrane comprising

positioning the nanomembrane and the metallic disk together atop the biological sample.

3. The method defined in claim 2, further comprising providing the nanomembrane with the

metallic disk lying thereon, flipping the nanomembrane so that the disk is underneath, the positioning

of the nanomembrane and the metallic disk being performed after the flipping of the nanomembrane.

4. A kit for use in making measurements of thermal diffusivity/conductivity of microscale

material, comprising: at least one nanomembrane having a maximum edge dimension in a microscale

range and at least one metallic disk having a maximum dimension substantially less than a smallest dimension of said at least one nanomembrane.

5. The kit defined in claim 4, comprising a plurality of nanomembranes each having a maximum edge dimension in a microscale range and further comprising a plurality of metallic disks each having a maximum dimension substantially less than a smallest dimension of each of said nanomembranes.

6. The kit defined in claim 5 wherein said disks are made of a material taken from the group consisting of gold, platinum, silver and aluminum and alloys thereof.

7. The kit defined in claim 5 wherein said disks are equal in number to said nanomembranes, each of said disks being fastened to a respective one of said nanomembranes.

8. A method for measuring thermal diffusivity/conductivity, comprising:

providing a microscale sample;

disposing a nanomembrane over the sample so that the nanomembrane and the sample are in thermal equilibrium with one another;

directing a laser beam to fall onto the nanomembrane over the sample;

operating a radiation sensor to detect photoluminescent radiation emitted by the nanomembrane in response to the laser beam;

determining a spectral shift in the detected photoluminescent radiation emitted by the nanomembrane; and

calculating thermal diffusivity/conductivity from the determined spectral shift of the photoluminescence.

9. The method defined in claim 8, further comprising placing a metallic disk between the nanomembrane and the sample prior to the directing of the laser beam to fall on the sample.

10. The method defined in claim 9 wherein the metallic disk is attached to the nanomembrane, the placing of the metallic disk and the disposing of the nanomembrane comprising positioning the nanomembrane and the metallic disk together atop the sample.

11. The method defined in claim 10, further comprising providing the nanomembrane with the metallic disk lying thereon, flipping the nanomembrane so that the disk is underneath, the positioning of the nanomembrane and the metallic disk being performed after the flipping of the nanomembrane.

12. The method defined in claim 9 wherein said disk is made of a material taken from the group consisting of gold, platinum, silver, aluminum and alloys thereof.

13. The kit defined in claim 9 wherein said disk is attached to said nanomembrane prior to the disposing a nanomembrane over the sample.
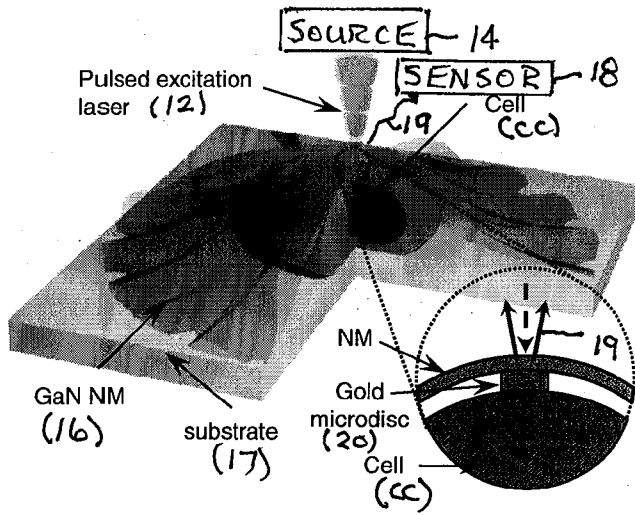
FIGURE 1
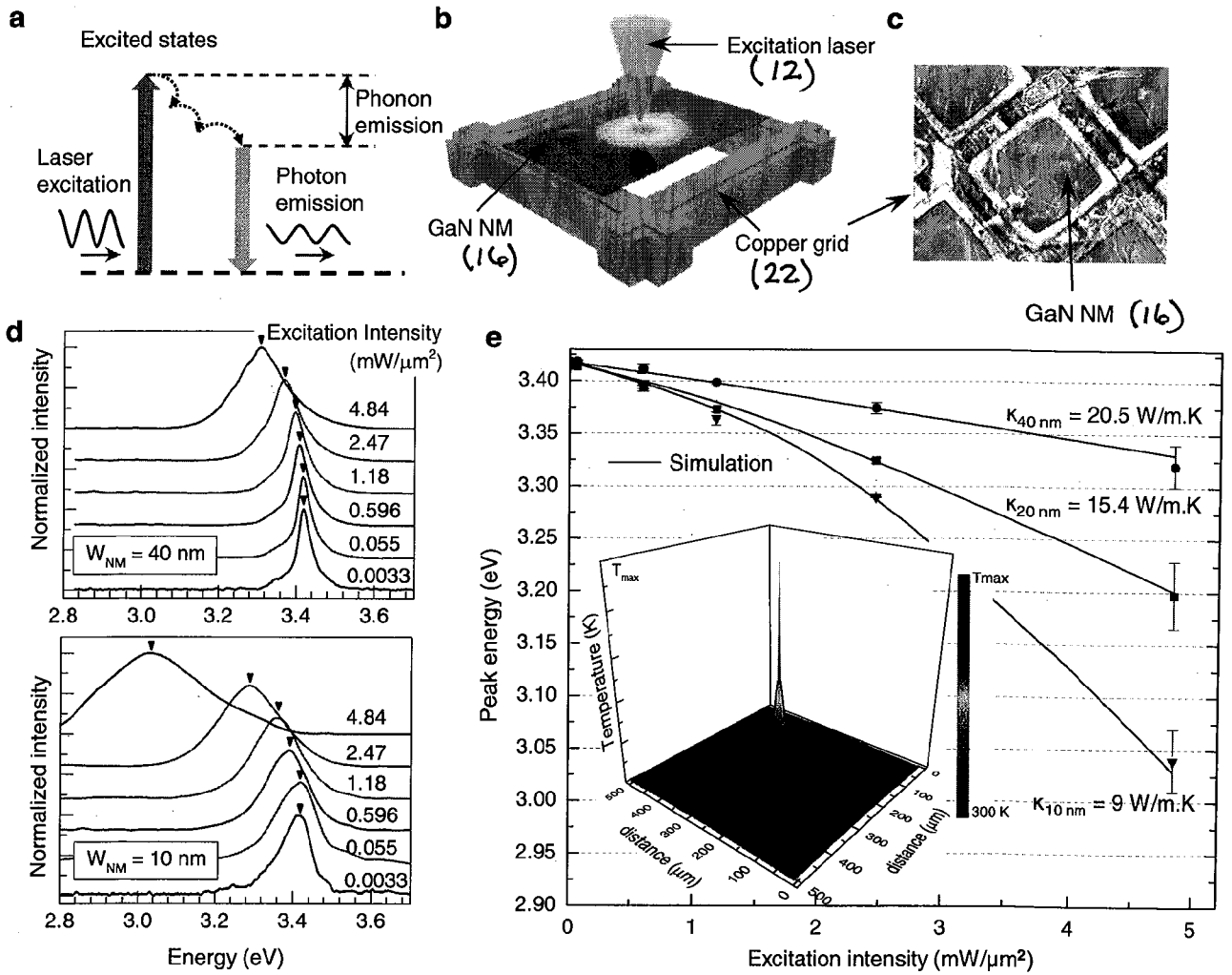
FIGURES 2a - 2e
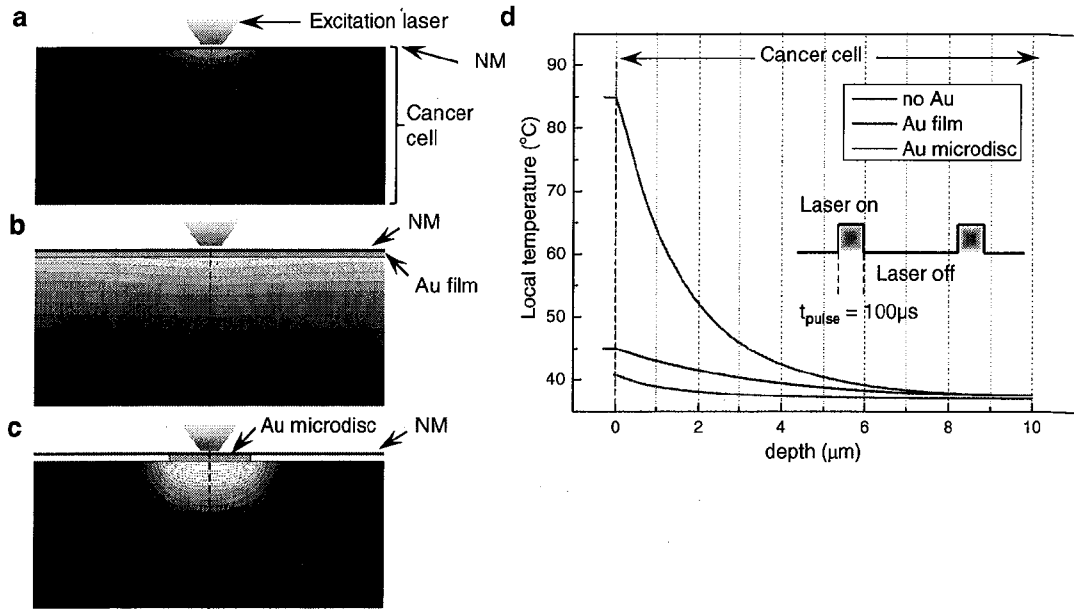
FIGURES 3a- 3d
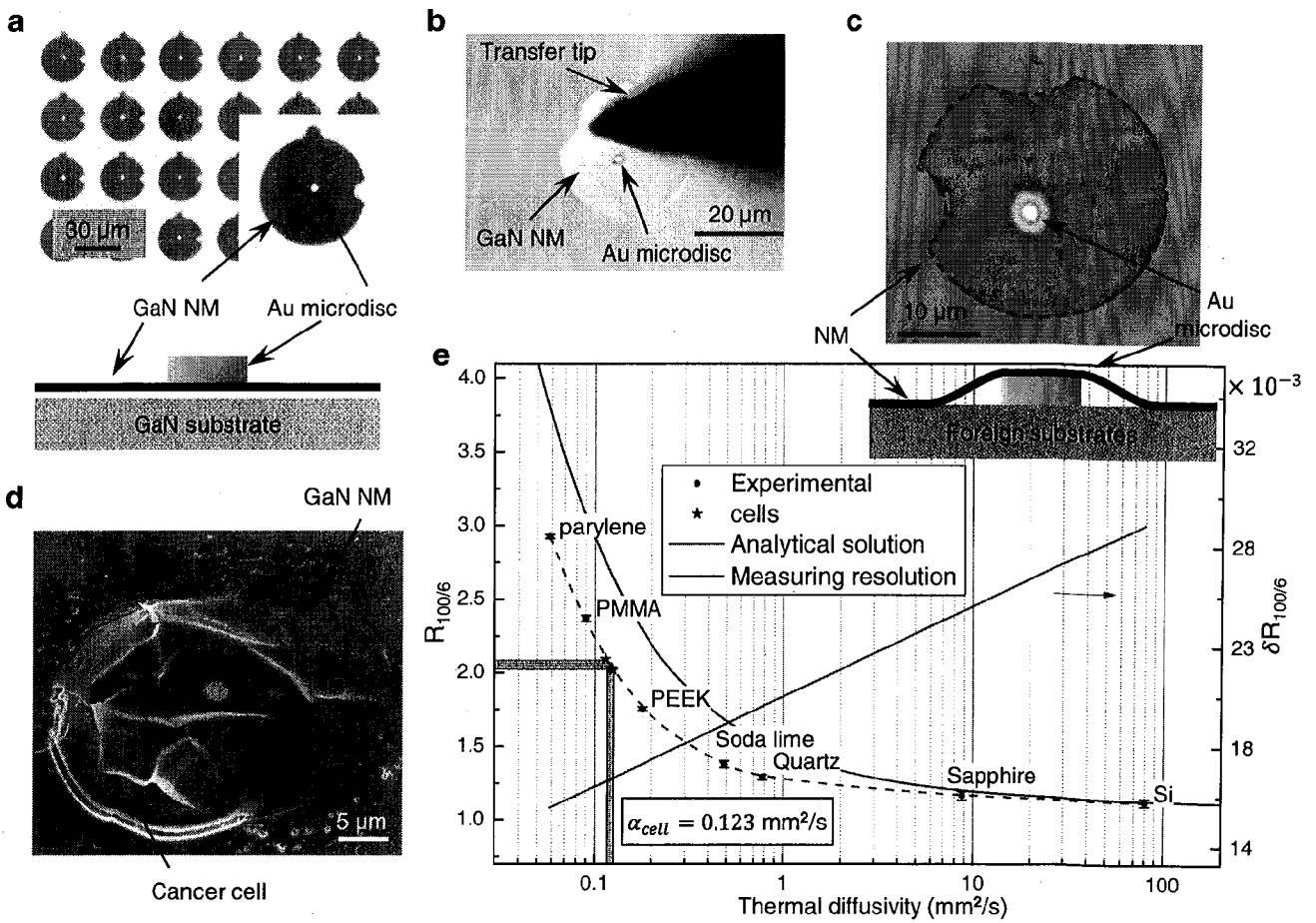
FIGURES 4a - 4e
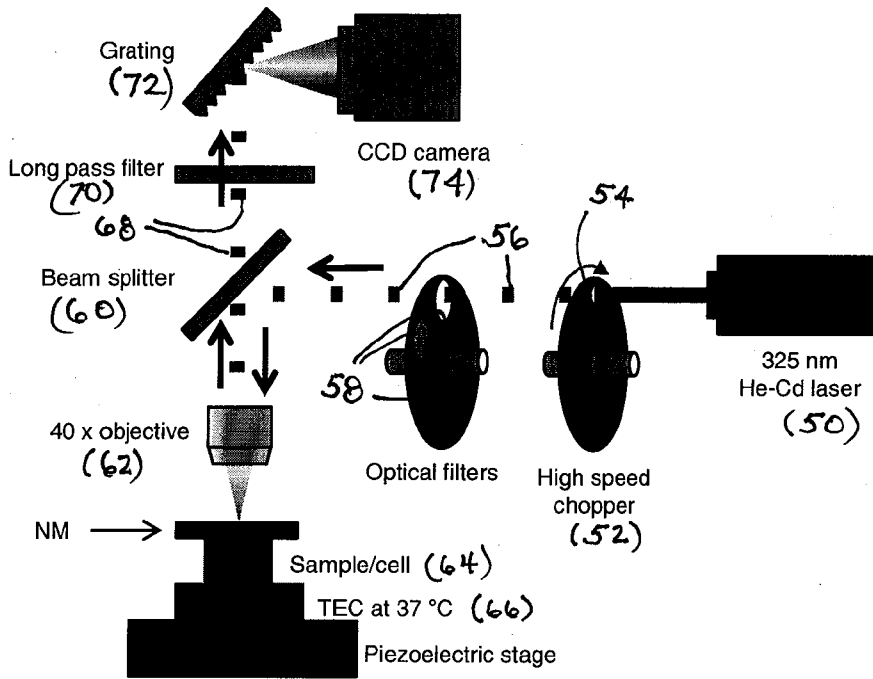
FIGURE 5
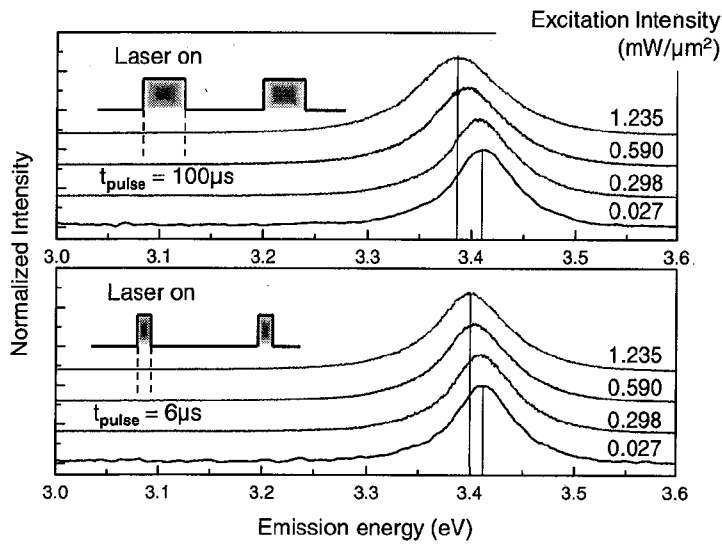
FIGURE 6

INTERNATIONAL SEARCH REPORT

International application No

PCT/IB2017/050269

A. CLASSIFICATION OF SUBJECT MATTER

INV. G01N33/50   G01N21/62   G01N25/18
ADD.

According to International Patent Classification (IPC) or to both national classification and IPC

B. FIELDS SEARCHED

Minimum documentation searched (classification system followed by classification symbols)

G01N

Documentation searched other than minimum documentation to the extent that such documents are included in the fields searched

Electronic data base consulted during the international search (name of data base and, where practicable, search terms used)

EPO-Internal, WPI Data, BIOSIS, EMBASE

C. DOCUMENTS CONSIDERED TO BE RELEVANT

Category*	Citation of document, with indication, where appropriate, of the relevant passages	Relevant to claim No.
A	Park: "Thermal conductivity of single biological cells and relation with cell viability: Applied Physics Letters: Vol 102, No 20", ; 1 May 2013 (2013-05-01), XP055356060, Retrieved from the Internet: URL:http://aip.scitation.org/doi/full/10.1 063/1.4807471 [retrieved on 2017-03-17] cited in the application abstract ----- -/--	1-13

[X] Further documents are listed in the continuation of Box C.   [ ] See patent family annex.

* Special categories of cited documents :

"A" document defining the general state of the art which is not considered to be of particular relevance

"E" earlier application or patent but published on or after the international filing date

"L" document which may throw doubts on priority claim(s) or which is cited to establish the publication date of another citation or other special reason (as specified)

"O" document referring to an oral disclosure, use, exhibition or other means

"P" document published prior to the international filing date but later than the priority date claimed

"T" later document published after the international filing date or priority date and not in conflict with the application but cited to understand the principle or theory underlying the invention

"X" document of particular relevance; the claimed invention cannot be considered novel or cannot be considered to involve an inventive step when the document is taken alone

"Y" document of particular relevance; the claimed invention cannot be considered to involve an inventive step when the document is combined with one or more other such documents, such combination being obvious to a person skilled in the art

"&" document member of the same patent family

Date of the actual completion of the international search	Date of mailing of the international search report
21 March 2017	31/03/2017

Name and mailing address of the ISA/	Authorized officer
European Patent Office, P.B. 5818 Patentlaan 2 NL - 2280 HV Rijswijk Tel. (+31-70) 340-2040, Fax: (+31-70) 340-3016	Gundlach, Björn

Form PCT/ISA/210 (second sheet) (April 2005)

C(Continuation).	DOCUMENTS CONSIDERED TO BE RELEVANT	
Category*	Citation of document, with indication, where appropriate, of the relevant passages	Relevant to claim No.
A	STONAS A R ET AL: "Development of selective lateral photoelectrochemical etching of InGaN/GaN for lift-off applications", APPLIED PHYSICS LETTERS, A I P PUBLISHING LLC, US, vol. 78, no. 13, 26 March 2001 (2001-03-26), pages 1945-1947, XP012027647, ISSN: 0003-6951, DOI: 10.1063/1.1352663 cited in the application figure 2 -----	1-13
X,P	Rami T. ElAfandy et al.: "Nanomembrane-Based, Thermal-Transport Biosensor for Living Cells - ElAfandy - 2016 - Small - Wiley Online Library", , 23 November 2016 (2016-11-23), XP055355925, Retrieved from the Internet: URL:http://onlinelibrary.wiley.com/doi/10.1002/smll.201603080/full [retrieved on 2017-03-17] the whole document -----	1-13